Chemically Reactive Oscillatory Casson Hybrid Nanofluid Flow with Heat Generation/Absorption Phenomenon Through Radiating Wavy Channel

B. Jaismitha and J. Sasikumar*

***Abstract*—Hybrid nanofluids, innovative colloidal suspensions of nanoparticles and base fluids, find extensive use in enhancing heat transfer efficiency in various industries, from electronics cooling to automotive engines. The present study examines the Chemical Reaction effect of Casson incompressible electrically conducting hybrid nanofluid with a heat source through a porous medium under the influence of an external magnetic field in an asymmetric wavy channel. $Cu - TiO_2$ nanoparticles are chosen for forming a hybrid water-based nanofluid. The flow problem is demonstrated in terms of PDEs with appropriate boundary conditions. The governing equations are solved and obtained analytical solution. Comparative results of skin friction coefficient and heat transfer rate for Cu-mixture ($Cu - SiO_2$, $Cu - TiO_2$ and $Cu - Al_2O_3$) are analysed. Graphs of velocity, temperature, and concentration profiles for various governing parameters are obtained to perceive the flow pattern perfectly.**

***Index Terms*—Chemical Reaction, Oscillatory flow, Heat Source, Porous medium, Casson fluid, Hybrid Nanofluid, MHD, Cu-Mixture**

I. Introduction

NANOFLUIDS have garnered considerable attention in various research studies aimed at enhancing heat transfer mechanisms. Numerous investigations have delved into the application of hybrid nanofluids to augment heat transfer in diverse engineering contexts, including but not limited to heat exchangers, food processing, energy storage systems, lubrication technologies, and the cooling of electronic devices. These specially engineered fluids, created through the fusion of metal nanoparticles, are commonly referred to as hybrid nanofluids. They exhibit remarkable improvements in thermal conductivity, rheological properties, and overall heat transfer characteristics. The emergence of nanofluids has opened up new horizons for both researchers and industrial practitioners. Subsequent advancements in nanotechnology have played a pivotal role in shaping contemporary manufacturing and technology landscapes. Hybrid nanofluids find wide-ranging applications across various industries and engineering disciplines, encompassing nuclear safety, microfluidics, manufacturing processes, transportation, military applications, pharmaceuticals, naval structures, acoustics, electro and biosensors, building systems, and the efficient cooling of flush-mounted electronic heaters in modern electronic devices and supercomputers. It was Choi [1](1995) who suggested the use of nanofluids to improve the thermophysical properties of working fluids. Compared to base fluids, he claimed that nanofluids had higher convective heat transfer coefficients, thermal diffusivity and thermal conductivity, which increases with an increase in volume fraction. Hasnain et al. [2] conducted a theoretical examination of how heat transfer enhancement occurs in an unsteady three-phase Casson fluid flow. This flow is confined by hybrid nanofluids along the walls of a horizontal channel. Madhesh et al. [3] analyzed the improvement of heat transport through a porous sandwich of hybrid and nanofluid in parallel plates. Naheeda Iftikhar et al. [4] looked at the features of several types of Nanoparticles(Nps) and the characteristics of the convective heat transfer effect with the peristaltic flow on continuous physiological delivery of MHD in a channel. The shrinking effect in a heterogeneous channel is discussed in $Cu - H_2O$ and $(Cu - SiO_2)H_2O$ hybrid nanoparticles(Hnps). When collating the data graphically for various forms, it is clear that the distribution of temperature and velocity curves is more vital in spherical shaped Nps compared to other shapes. Gul Aizar et al. [5] examined the effects of thermal radiation and heat transfer rate in mixed convection MHD flow of ethylene glycol (EG) and water-based nanofluids containing various shapes of alumina nanoparticles. It was discovered that blade-shaped nanoparticles and brick-shaped nanoparticles move slower than cylindrical-shaped nanoparticles.

To gain a full understanding of non-Newtonian fluids and their numerous applications, it is essential to analyze their flow behavior. Non-Newtonian fluid flow has received a great deal of attention in the field of fluid mechanics due to its usefulness in industry and technology. Engineers, physicists, and mathematicians face challenges when dealing with non-Newtonian fluid mechanics like non-linearity, including food drilling operations and bio-engineering. Casson fluid is a non-Newtonian fluid model. In the literature, it has been stated that the Casson fluid model is more accurate at reflecting rheological data than a conventional viscoelastic model. Casson fluid can be found in jelly, tomato sauce, honey, soup, and concentrated fruit liquids. A number of factors can explain why Casson fluid is similar to human blood due to its aqueous base plasma composition, which contains various components such as proteins, fibrinogen, and globulin, all of which are present in human blood. A chain-like structure that is formed in human blood cells is

Manuscript received January 24, 2023; revised September 26, 2023.

B. Jaismitha is a research Scholar, Department of Mathematics, College of Engineering and Technology, Faculty of Engineering and Technology, SRM Institute of Science and Technology, SRM Nagar, Kattankulathur-603203, Chengalpattu District, Tamil Nadu, INDIA e-mail:jb1645@srmist.edu.in.

*J. Sasikumar is an Assistant Professor at Department of Mathematics, College of Engineering and Technology, Faculty of Engineering and Technology, SRM Institute of Science and Technology, SRM Nagar, Kattankulathur-603203, Chengalpattu District, Tamil Nadu, INDIA (corresponding author to provide email:sasikumj@srmist.edu.in)

known as aggregate rouleaux. In the case of rouleaux acting as plastic solids, yield stress occurs that corresponds to the constant yield of Casson fluid in rouleaux [6]-[10]. Eldabe et al. [11] investigated the heat transfer between rotating cylinders of an incompressible electrically conducting Casson fluid. Swati Mukhopadhyay et al. [12] studied numerical solutions for unsteady Casson fluid boundary layer flow and heat transfer rate over-stretching surfaces. It is to be noted that an increase in the unsteadiness parameter causes a drop in fluid velocity, and the temperature drops dramatically as well. Increasing Casson parameter values reduces the velocity and maximizing it enhances the temperature. Hari R. Kataria and Patel [13] examined the exact solution to the time-dependent highly viscous Casson fluid flow that convection occurs through an oscillating erect plate in the presence of thermal radiation, chemical reaction, Soret effect, and heat generation through a permeable medium. Jithender Reddy et al. [14] examined the time-dependent magnetohydrodynamic mechanisms involved in heat transfer and viscous dissipation flow of highly viscous Casson fluid over an oscillating plate with emergent values. The effect of MHD and porosity of mixed convection of Casson hybrid nanofluid $Cu - Al_2O_3$ in sodium alginate base fluid is analysed by Sidra Aman et al. [15] and it is noted that the temperature is enhanced with an increase in thermal radiation. Velocity rises with an increase in Gr, k, and falls with an increase in the Hartmann number. Zahir Shah et al. [16] looked at entropy optimization in electrically conducting Casson nanofluid on a non-linear stretchy surface. Yaqing Liu et al. [17] consider the MHD flow of an incompressible generalized Oldroyd-B fluid. According to Zainal Abdul Aziz et al. [18], the magnetohydrodynamic (MHD) and rotating flow of a generalized Burgers fluid over a variable-accelerated plate has an exact steady-state solution. This investigation employed the Fourier sine transform technique to obtain the solution. The results were subsequently expressed in various equivalent forms using exponential, sine, and cosine functions. Notably, the present exact solution can also be applied to other fluid models, including Burgers, Oldroyd-B, Maxwell, second grade, and Navier-Stokes. References [19] - [24]. provide some relevant studies on the topic.

According to Shipra Mital and Tripathi Manajo [25], the development of impurity energy levels inhibits charge recombination and extends photosensitivity to the visible range. TiO_2 is expected to see new industrial applications in the future. The continuous rise in the photocatalytic characteristics of TiO_2 results in surface modification and will enable the photocatalyst to reach its full potential in the future. A study carried out by Ali Chamkha et al. [26] investigated and graphically illustrated the results of stable laminar boundary flow of both natural and forced convection around a vertical cone of nanofluid. Hamilton and Crosser [27] have investigated the thermal conductivities of a wide range of heterogeneous mixtures of two components, both theoretically and experimentally. In a time-dependent boundary condition, Olumioel and Makinde et al. [28] investigated the effect of slip on hydromagnetic pulsatile flow through a channel filled with permeable media. Zin et al. [29] explored the tribological characterisation of various nano lubricants and published their findings. A variety of nanoparticles, including copper, titanium oxide and carbon nanostructures, were used to investigate the impact of nanoparticle size and chemical nature on the performance of nano-oil in various lubrication regimes. In the presence of an asymmetric wavy channel, P. V. Sathya Narayana et al. [30] investigated the effect of heat source and chemical reaction on MHD oscillatory fluid flow. J. Sasikumar and A. Govindarajan [31] investigated the effect of slip in MHD oscillatory fluid in an asymmetric wavy channel. In a study conducted by S. Asghar et al. [32], the flow of a third-grade fluid across a permeable plate oscillating simultaneously with injection and suction for amplitudes of different parameters was studied. Makinde and P.Y. Mohone [33] investigated the phenomenon of unsteady flow of conducting thin fluid through a rectangular channel within permeable materials under heat transfer and transverse magnetic fields. Based on an analysis conducted by W. N Mutuku [34], various shapes of Al_2O_3 and TiO_2 nanoparticles were incorporated into an ethylene glycol-based nanofluid to study its cooling characteristics. According to [35], J. Sasikumar et al. studied oscillatory flow in a porous medium inside a rotating wavy channel by investigating the effects of MHD and fluid viscosity. They presented graphical representations of velocity, temperature, and concentration distributions. J. Sasikumar et al. [36] analysed the effect of velocity slip, thermal radiation and chemical reaction on MHD oscillatory flow through an irregular channel. J. Sasikumar et al. [37] analysed the MHD viscous oscillating type blood flow through the lumen in arteries and varicose veins and analysed the impact of viscous dissipation and chemical reactions on blood flow. MHD oscillatory flow has been studied in various fields in references [38] - [46].

From the above literature overview, the study examines the heat generation/absorption and chemical reaction effect of Casson incompressible electrically conducting hybrid nanofluid through a porous medium under the influence of an external magnetic field in an asymmetric wavy channel. $Cu - TiO_2$ nanoparticles are considered with water-based fluid. A comparative study of the skin friction coefficient and heat transfer rate for $Cu - SiO_2$, $Cu - TiO_2$ and $Cu - Al_2O_3$ in water based-nanofluid is conducted. The governing equations are solved analytically and effects of various important parameters on the velocity, temperature and concentration profiles are sketched and discussed.

II. Mathematical Formulation of the Problem

Consider the flow phenomenon of the problem to be 2D incompressible, chemically reacting, electrically conducting Casson hybrid $(Cu - TiO_2)/H_2O$ nanofluid with heat generation/absorption through an asymmetric wavy channel.

The rheological equation of state for an isotropic and incompressible flow of a Casson fluid is seen in ref.[12]

$$\tau_{ij} = 2(\mu_B + P_y/\sqrt{2\pi})e_{ij} \ ,\pi > \pi_c$$

$$2(\mu_B + P_y/\sqrt{2\pi})e_{ij} \ ,\pi < \pi_c$$

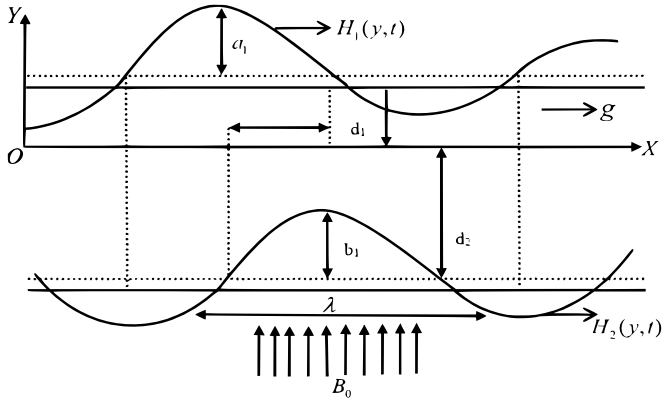

Fig. 1: Physical model of the problem.

TABLE I: Thermophysical properties of water (basefluid) and nanoparticles[5].

Model	$\rho\left(kg/m^3\right)$	$c_p(J/kgK)$	$k(W/mK)$	$\beta \times 10^{-5}$
H_2O	997.1	4179	0.613	21
Cu ϕ_1	8933	385	400	1.67
TiO_2 ϕ_2	4250	686.2	8.9528	0.9
Al_2O_3	3940	765	40	0.85
SiO_2	2220	745	1.4	5.5

τ_{ij} represents the stress tensor's (i, j)-th component, while π is calculated as $e_{ij}e_{ij}$, with e_{ij} representing the (i, j)-th component of the deformation rate. π signifies the squared magnitude of the deformation rate components, and π_c serves as a critical value for this product according to the non-Newtonian model. Additionally, μ_B denotes the plastic dynamic viscosity specific to the non-Newtonian fluid, and P_y stands for the fluid's yield stress. If the applied shear stress to the fluid is less than the yield stress (P_y), the fluid behaves as a solid. Conversely, if the applied shear stress exceeds the yield stress, the fluid exhibits a flowing behavior.

Channel Wall Equations:-

$$\begin{aligned} \mathrm{H}_1 &= d_1 + a_1 cos\tfrac{2\pi x}{\lambda} \\ H_2 &= -d_2 - b_1 cos(\tfrac{2\pi x}{\lambda} + \phi) \end{aligned} \tag{1}$$

Where a_1, b_1, d_1, d_2 and ϕ satisfy the condition $a_1^2 + b_1^2 + 2a_1b_1cos\phi \leq (d_1 + d_2)^2$.

The oscillation occurs within the phase difference denoted as ϕ, which falls within the range of $0 \leq \phi \leq \pi$. Radiative heat transfer is facilitated by the channel walls' maintaining T_1 and T_2 temperatures, both of which are sufficiently high to facilitate the transfer of heat. Induced magnetic fields are believed to be negligible because the Reynolds number is so small and the magnetic field is applied transversely. The oscillation of fluid is brought about by an oscillating pressure gradient applied across the channel ends and an asymmetric wavy channel configuration. While keeping the constant value of k_1, we consider the factors of viscous resistance and Darcy's resistance. The governing equations for momentum, energy, and concentration are as follows: -

$$\rho_{hnf}\tfrac{\partial u}{\partial t} = -\tfrac{\partial p}{\partial x} + \mu_{hnf}(1 + \tfrac{1}{\beta})\tfrac{\partial^2 u}{\partial y^2} - (\sigma_{hnf}B_0^2 + \tfrac{\mu_{hnf}}{k_1})u$$

$$+(\rho\beta_T)_{hnf}g(T - T_0) + (\rho\beta_c)_{hnf}g(C - C_0), \tag{2}$$

$$(\rho c_p)_{hnf}\frac{\partial T}{\partial t} = k_{hnf}\frac{\partial^2 T}{\partial y^2} + \frac{\partial q}{\partial y} + Q_0(T - T_0) \tag{3}$$

$$\frac{\partial C}{\partial t} = D_{hnf}\frac{\partial^2 C}{\partial y^2} - Kr(C - C_0) \tag{4}$$

the radiative heat flux:

$$\frac{\partial q}{\partial y} = 4\alpha^2(T - T_0) \tag{5}$$

The boundary conditions are as follows:

$$\begin{aligned} &u = 0 \quad T = \mathrm{T}_1 \qquad \mathrm{C} = C_1 \qquad \text{on} \quad \mathrm{y} = \mathrm{H}_1, \\ &u = 0 \quad T = \mathrm{T}_0 + (T_0 - T_1)e^{i\omega t} \quad \mathrm{C} = C_0 + (C_0 - C_1)e^{i\omega t} \text{on} \\ &\mathrm{y} = \mathrm{H}_2. \end{aligned} \tag{6}$$

Where u= u(y, t), T= T(y, t), C= C(y, t), ρ_{hnf}, μ_{hnf}, σ_{hnf}, β_T, β_c, g, $(\rho c_p)_{hnf}$, k_{hnf}, α_0, D_{hnf} are respectively fluid velocity in the x-direction, temperature, concentration, density, dynamic viscosity, electrical conductivity of the base fluid, volumetric thermal expansion coefficient, gravitational acceleration, heat capacitance of nanofluids, thermal conductivity of nanofluid, radiation absorption and thermal diffusion coefficient.

In this study, the $(\rho\beta)_{hnf}$, μ_{hnf}, $(\rho c_p)_{hnf}$, k_{bf} and k_{hnf} are considered here to analyze both spherical and non-spherical shaped nanoparticles.

$$(\rho\beta)_{hnf} = (1 - \phi_2)(\rho\beta)_f\left[(1 - \phi_1) + \phi_1\left(\tfrac{(\rho\beta)_{s1}}{(\rho\beta)_f}\right)\right] + \phi_2(\rho\beta)_{s2},$$

$$\mu_{hnf} = \tfrac{\mu_f}{(1-\phi_2)^{2.5}(1-\phi_1)^{2.5}},$$

$$(\rho c_p)_{hnf} = (1 - \phi_2)(\rho c_p)_f\left[(1 - \phi_1) + \phi_1\left(\tfrac{(\rho c_p)_{s1}}{(\rho c_p)_f}\right)\right] + \phi_2(\rho c_p)_{s2},$$

$$\begin{aligned} k_{hnf} &= \left(\tfrac{k_{s2}+(n-1)k_{bf}-(n-1)\phi_2(k_{bf}-k_{s2})}{k_{s2}+(n-1)k_{bf}+\phi_2(k_{bf}-k_{s2})}\right)k_{bf}, \\ k_{bf} &= \left[\tfrac{k_{s1}+(n-1)k_f-(n-1)\phi_1(k_f-k_{s1})}{k_{s1}+(n-1)k_f+\phi_1(k_f-k_{s1})}\right]k_f, \end{aligned} \tag{7}$$

where ϕ_1, ϕ_2, are the nanoparticles volume fraction, ρ_f, ρ_{s1}, and ρ_{s2} is the density of the base fluid and hybrid nanoparticles, the volumetric coefficient of thermal expansions of nanoparticles and base fluids are denoted by β_{s1}, β_{s2}, and β_f respectively, $(c_p)_{s1}, (c_p)_{s2}$ and $(c_p)_f$ are the specific heat capacities of nanoparticles and base fluids at constant pressure. Here k_{s1}, k_{s2} and k_f are thermal conductivities of nanoparticles and base fluid.

We introduce the following non-dimensional quantities.

$$u^* = \frac{u}{U_0}, \quad x^* = \frac{x}{d}, \quad t^* = \frac{tU_0}{d}, y^* = \frac{y}{d}, \quad p^* = \frac{d}{\mu U_0}p,$$
$$Kr = \frac{dk_r}{U}, \lambda_0^* = \frac{\lambda_0 d^2}{\mu U_0}, \lambda^* = \frac{\lambda d^2}{\mu U_0}, Sc = \frac{\nu_{hnf}}{D_{hnf}}, Re = \frac{U_0 d}{\nu_{hnf}},$$
$$Gr = \frac{g\beta_{hnf} d^2 (T_w - T_0)}{\nu_{hnf} U_0}, k = \frac{k_1}{d^2}, \theta = \frac{T-T_0}{T_d - T_0}, \quad a = \frac{a_1}{d_1},$$
$$C^* = \frac{C-C_0}{C_d - C_0}, \quad \omega^* = \frac{\omega d}{U_0}, \quad d = \frac{d_2}{d_1}, \quad b = \frac{b_1}{d_1}, Q = \frac{Q_H d^2}{k}$$
$$N^2 = \frac{4d^2\alpha^2}{k_f}, \quad M^2 = \frac{\sigma B_0^2 d^2}{\mu_{hnf}}, \quad Pe = \frac{U_0 d (\rho c_p)_{hnf}}{k_{hnf}},$$
$$Gc = \frac{g\beta_{hnf} d^2 (C_w - C_0)}{\nu_{hnf} U_0} \tag{8}$$

The boundary conditions in non-dimensional form become $h_1 = 1 + a\cos 2\pi x$ and $h_2 = -d - b\cos(2\pi x + \varphi)$ where a, b, d and φ satisfy the condition $a^2 + b^2 + 2ab\cos\varphi(1+d)^2$.

The following non-dimensional differential Equations are obtained (asterisk* is omitted for convenience).

$$\psi_1 Re \frac{\partial u}{\partial t} = \lambda e^{i\omega t} + \psi_2 (1 + \frac{1}{\beta}) \frac{\partial^2 u}{\partial y^2} - (M + \frac{\psi_2}{k}) u + \psi_3 Gr\theta + \psi_4 GmC, \tag{9}$$

$$\psi_5 \frac{Pe}{\lambda_{hnf}} \frac{\partial \theta}{\partial t} = \frac{\partial^2 \theta}{\partial y^2} + \frac{N^2}{\lambda_{hnf}}\theta + \frac{Q}{\lambda_{hnf}}\theta, \tag{10}$$

$$\frac{Sc}{(1-\phi_1)(1-\phi_2)} \frac{\partial C}{\partial t} = \frac{\partial^2 C}{\partial y^2} - KrC. \tag{11}$$

The corresponding boundary conditions in nondimensional form are as follows:

$$\begin{array}{llll} u = 0 & \theta = 0 & C = 0 & on \quad y = h_1, \\ u = 0 & \theta = e^{i\omega t} & C = e^{i\omega t} & on \quad y = h_2. \end{array} \tag{12}$$

where,

$$\psi_1 = (1-\phi_2)\left[(1-\phi_1) + \phi_1 \frac{\rho_{s1}}{\rho_f}\right] + \phi_2 \frac{\rho_{s2}}{\rho_f},$$
$$\psi_2 = \frac{\mu_f}{(1-\phi_2)^{2.5}(1-\phi_1)^{2.5}},$$
$$\psi_3 = \left\{(1-\phi_2)\left[(1-\phi_1) + \phi_1\left(\frac{(\rho\beta_T)_{s1}}{(\rho\beta_T)_f}\right)\right] + \phi_2 \frac{(\rho\beta_T)_{s2}}{(\rho\beta_T)_f}\right\},$$
$$\psi_4 = \left\{(1-\phi_2)\left[(1-\phi_1) + \phi_1\left(\frac{(\rho\beta_c)_{s1}}{(\rho\beta_c)_f}\right)\right] + \phi_2 \frac{(\rho\beta_c)_{s2}}{(\rho\beta_c)_f}\right\},$$
$$\psi_5 = \left\{(1-\phi_2)\left[(1-\phi_1) + \phi_1\left(\frac{(\rho c_p)_{s1}}{(\rho c_p)_f}\right)\right] + \phi_2 \frac{(\rho c_p)_{s2}}{(\rho c_p)_f}\right\},$$
$$\lambda_{hnf} = \frac{k_{hnf}}{k_{bf}}, \tag{13}$$

A. METHOD OF SOLUTION

The partial differential equations of velocity, temperature, and concentration profile are converted to an ordinary differential equation using Eq (13) by taking the pressure gradient purely oscillatory

$$u(y,t) = u_0(y)e^{i\omega t},$$
$$\theta(y,t) = \theta_0(y)e^{i\omega t},$$
$$C(y,t) = C_0(y)e^{i\omega t},$$
$$-\frac{\partial p}{\partial x} = \lambda e^{i\omega t}. \tag{14}$$

III. CALCULATIONS

Substituting Eq (13) into Eqs (9) -(11), we obtain.

$$l^2 \frac{d^2 u_0}{dy^2} - s^2 u_0 = -\lambda - \phi_3 Gr\theta_0 - \phi_4 GcC_0, \tag{15}$$

$$\frac{d^2\theta_0}{dy^2} + p^2\theta_0 = 0, \tag{16}$$

$$\frac{d^2 C_0}{dy^2} + r^2 C_0 = 0. \tag{17}$$

In non-dimensional form, the associated boundary conditions are as follows:

$$\begin{array}{llll} u_0 = 0 & \theta_0 = 0 & C_0 = 0 & on \quad y = h_1, \\ u_0 = 0 & \theta_0 = 1 & C_0 = 1 & on \quad y = h_2. \end{array} \tag{18}$$

Solving equations (14) – (16) under the boundary conditions (17), the expression for velocity, temperature and concentration is as follows:

$$u(y,t) = -A_1 e^{((s/l)(y-h_2))} + B_1 + C_1\left[\frac{sinp(y-h_2)}{sinp(h_1-h_2)}\right] + C_1\left[\frac{sinhr(h_2-y)}{sinhr(h_2-h_1)}\right] - \left[\frac{A_1+B_1+C_1-A_1 e^{((s/l)(y-h_2))}}{sinh(s/l)(h_1-h_2)}\right] sinh(s/l)(y-h_2)]e^{i\omega t} \tag{19}$$

$$\theta(y,t) = \frac{sinp(y-h_2)}{sinp(h_1-h_2)} e^{i\omega t} \tag{20}$$

$$C(y,t) = \frac{sinhr(h_2-y)}{sinhr(h_2-h_1)} e^{i\omega t} \tag{21}$$

The Skin Friction Coefficient across the channels wall is given by

$$\tau = (1 + \frac{1}{\beta})(\frac{\partial u}{\partial y})_{h_1, h_2} =$$
$$(1 + \tfrac{1}{\beta})\ [-A_1 e^{((s/l)(y-h_2))}(\tfrac{s}{l}) + B_1 + C_1 p[\frac{cosp(y-h_2)}{sinp(h_1-h_2)}] + C_1 r[\frac{coshr(h_2-y)}{sinhr(h_2-h_1)}] - [\frac{A_1+B_1+C_1-A_1 e^{((s/l)(y-h_2))}}{sinh(s/l)(h_1-h_2)}] cosh(s/l)(y-h_2)(\tfrac{s}{l})]e^{i\omega t} \tag{22}$$

The Rate of heat transfer across the walls of the channel is given by

$$Nu = -(\frac{\partial \theta}{\partial y})_{h_1,h_2} = \frac{-pcosp(y-h_2)}{sinp(h_1-h_2)} e^{i\omega t} \quad (23)$$

The rate of mass transfer across the channels wall is given by

$$Sh = -(\frac{\partial C}{\partial y})_{h_1,h_2} = \frac{rsinhr(h_2-y)}{sinhr(h_2-h_1)} e^{i\omega t} \quad (24)$$

All the above constants of equations (14)-(23) are given in Appendix .

IV. RESULTS AND DISCUSSIONS

A. Discussion of graphical results

In this investigation, the chemical reaction effect and heat generation/absorption phenomena on MHD oscillatory Casson hybrid NFs flow in an asymmetric channel in the presence of a magnetic field parameter is analysed for various flow parameters and the graphs of velocity, temperature and concentration distribution for hybrid nanofluids are obtained using MATLAB software. The graphs are presented using the thermophysical properties for base fluid and nanofluid from Table I. The below-given figures demonstrate the impact of physical parameters like Magnetic field M, Grashof number Gr, radiation parameter N, frequency parameter ω, Permeability parameter k, and β Casson parameter. In these calculations, we consider t = 0.1, Pe = 10, Gr = 1, Gc = 1, Sc = 1, N = 1, Kr = 1, k = 1, $\beta = 2$, M = 1, $\omega = \pi/4$, λ = 1, while other parameters are varied over a range which is listed in figure captions.

In Fig 2, the velocity distribution for various magnetic field parameter values is observed. It is noticed that the strong magnetic field affects the velocity. This happens because the Lorentz force generated as a result of the magnetic field strength is dominated by the viscous force in the flow direction; therefore, the velocity decreases. This result goes on line with [34]. The velocity distribution for different values of chemical reaction parameter Kr is analysed in Fig 3. It is obvious from the figure that the velocity decreases with an increase in the values of the chemical reaction parameter. The above results go on line with [31]. Fig 4 indicates that the effect of various values of the Casson parameter in velocity distribution is depicted. It is found that β when is increased, the velocity decreases. In Fig 5, various values of the Grashof number in the velocity profile have been analysed. It is observed that the velocity profile is enhanced with an increase in the Grashof number. Physically, when the Grashof number is increased, the temperature gradient will be produced, which leads to buoyancy force, and therefore velocity is increased. This result has been confirmed with the outcome of Makinde and Mhone [34].

The Fig 6 describes the velocity profile for various values of thermal radiation parameters. It is observed that increase in the thermal radiation parameter increases, which means the heat energy transferred to the fluid enhances the velocity. The velocity profile for various values of permeability parameter k is analysed in Fig 7. It is observed the values of the permeability parameter enhance the

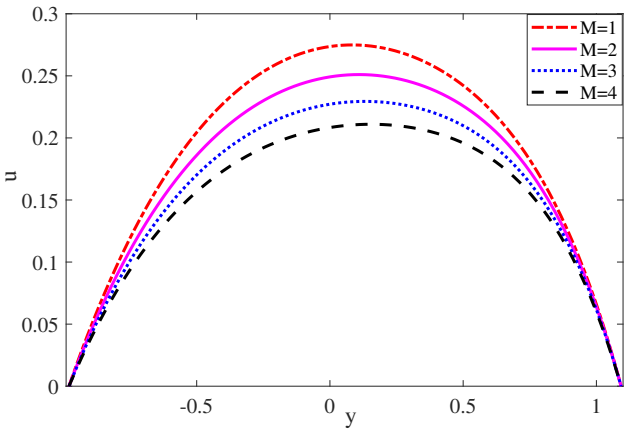

Fig. 2: Velocity distribution for different values of M when t= 0.1, Pe= 10, Gr= 1, Gc= 1, N= 1, Kr= 1,k= 1, $\beta = 2$, $\omega = \pi/4$,λ= 1, $Re = 1$, $Q = 1$.

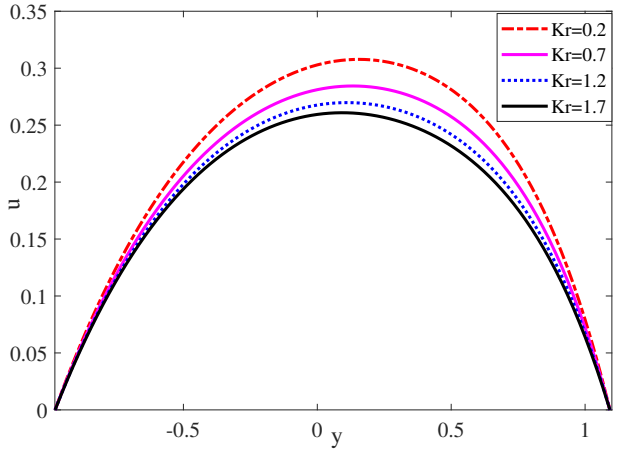

Fig. 3: Velocity distribution for different values of Kr when t= 0.1, Pe= 10, Gr= 1, Gc= 1, N= 1, M= 1, k= 1, $\beta = 2$, $\omega = \pi/4$, λ= 1, Sc=1, $Re = 1$, $Q = 1$.

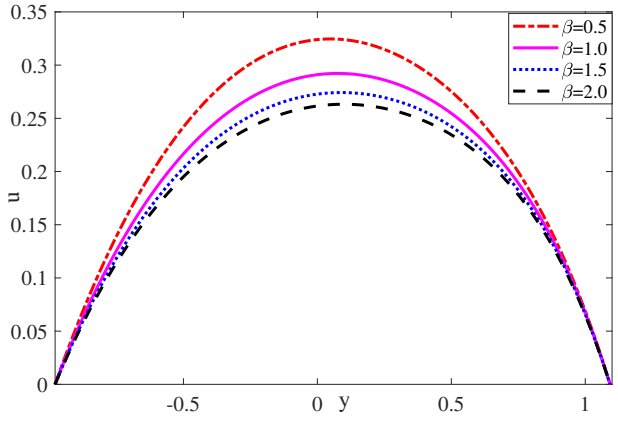

Fig. 4: Velocity distribution for different values of β when t= 0.1, Pe= 10, Gr= 1, Gc= 1, N= 1, Sc=1, Kr= 1,k= 1, M= 1, $\omega = \pi/4$, λ= 1, $Re = 1$, $Q = 1$.

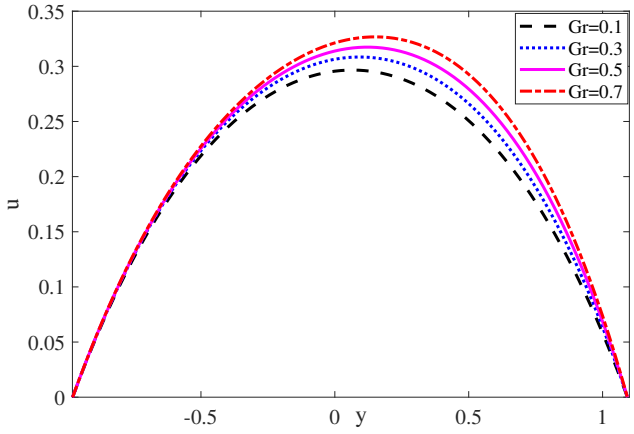

Fig. 5: Velocity distribution for different values of Gr when t= 0.1, Pe= 10, M= 1, Sc=1, Gc= 1, N= 1, Kr= 1, k= 1, $\beta = 2$, $\omega = \pi/4$, $\lambda = 1$, $Re = 1$, $Q = 1$.

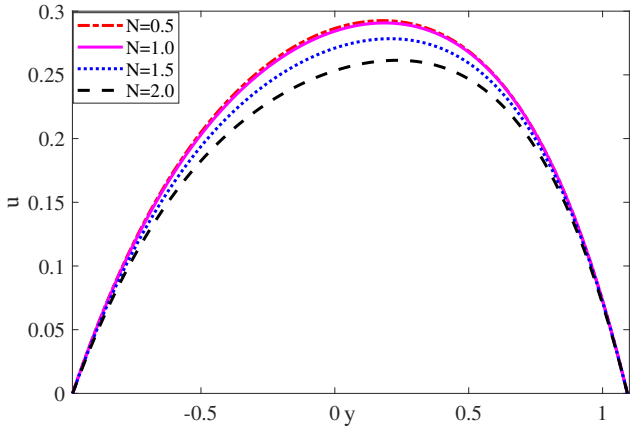

Fig. 6: Velocity distribution for different values of N when t= 0.1, Pe= 10, Gr= 1, Gc= 1, M= 1, Kr= 1, k= 1, $\beta = 2$, $\omega = \pi/4$, $\lambda = 1$, $Re = 1$, $Q = 1$.

velocity, which is due to Darcy's law. Physically, as the fluid has less frictional force when k increases, velocity also increases. These results agree with Gul Aaiza et al. [5]. Fig 8 shows that the velocity profile decreases with the increasing influence of the Reynolds number. The below-given graphs demonstrate the temperature and concentration distribution. The impact for various values of thermal radiation parameter, oscillatory parameter, Peclet number, chemical reaction parameter and Volume fraction.

In Fig 9 and Fig 10, the temperature profile for various values of thermal radiation parameter and Peclet number in $CuTiO_2/H_2O$ hybrid nanofluid is analysed. It is observed that for all values of the thermal radiation parameter, the temperature decreases till y = 0 and gradually temperature increases for all values of N. This depicts that the fluid has more energy transfer. For all values of the Peclet number, the temperature decreases till y = 0 and gradually, an increase is observed for all values of Pe.

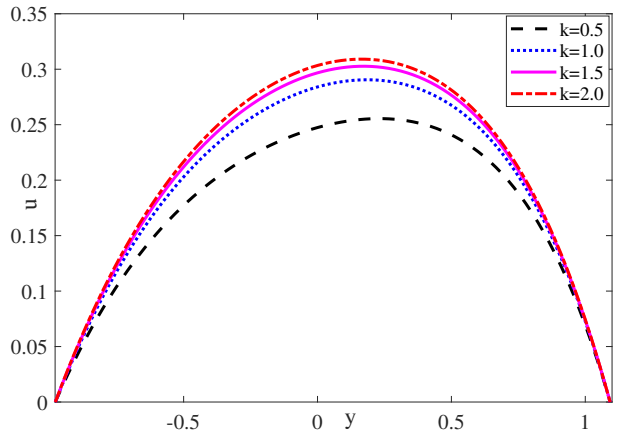

Fig. 7: Velocity distribution for different values of k when t= 0.1, Pe= 10, Gr= 1, Gc= 1, M= 1, Kr= 1, M= 1, $\beta = 2$, $\omega = \pi/4$, $\lambda = 1$, $Re = 1$, $Q = 1$.

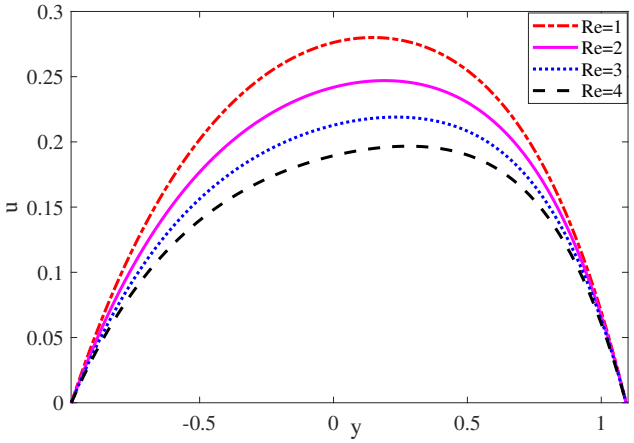

Fig. 8: Velocity distribution for different values of Re when t= 0.1, Pe= 10, Gr= 1, Gc= 1, M= 1, Kr= 1, k= 1, $\beta = 2$, $\omega = \pi/4$,$\lambda = 1$, $M = 1$, $Q = 1$.

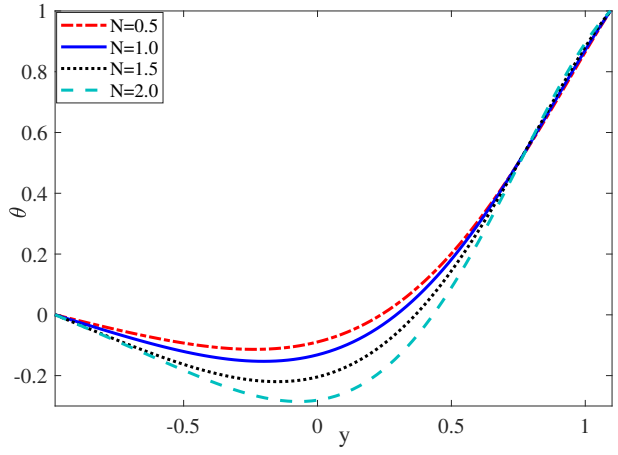

Fig. 9: Temperature distribution for different values of N when t= 0.1, Pe= 10, Q=1, N= 1, $\phi_1 = 0.04$, $\phi_2 = 0.04$.

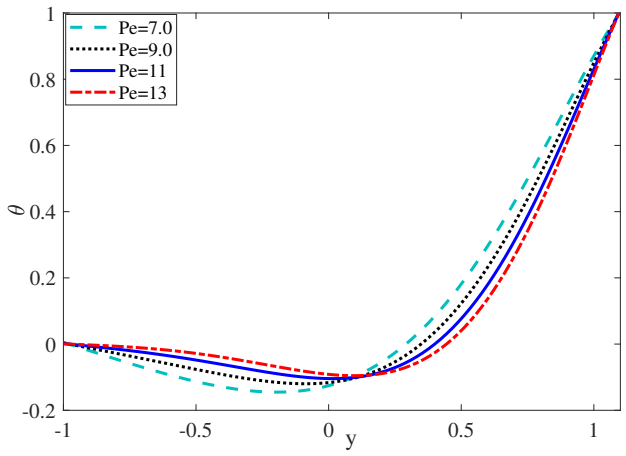

Fig. 10: Temperature distribution for different values of Pe when t= 0.1, N= 1, ω= $\pi/4$, Q= 1,$\phi_1 = 0.04$, $\phi_2 = 0.04$.

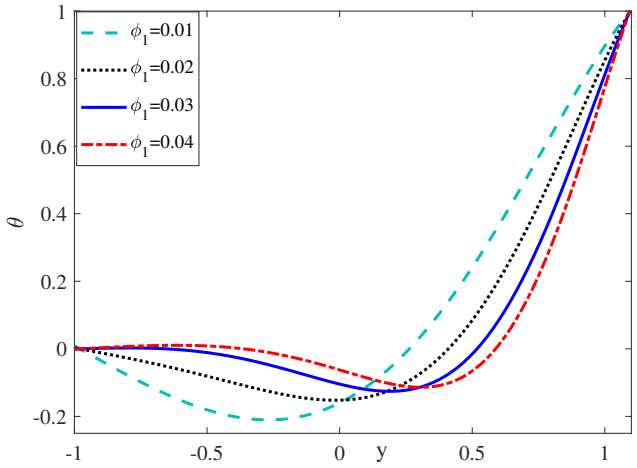

Fig. 11: Temperature distribution for different values of ϕ_1 when t= 0.1, Pe= 10, N= 1, $\beta = 2$, $Q = 1$, $\phi_1 = 0.04$, $\phi_2 = 0.04$.

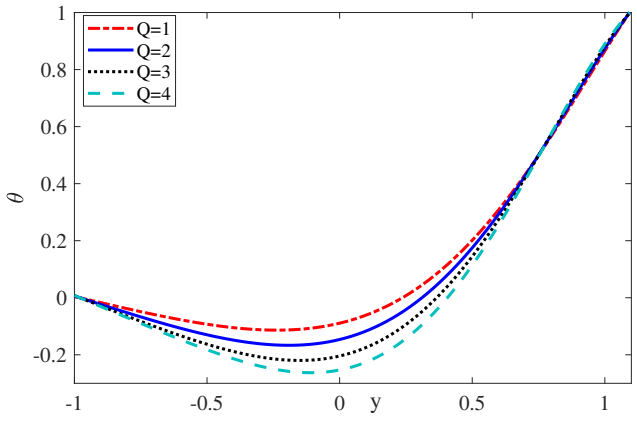

Fig. 12: Temperature distribution for different values of heat source when t= 0.1, Pe= 10, N= 1, $\beta = 2$, λ= 1, Q= 1, $\phi_1 = 0.04$, $\phi_2 = 0.04$

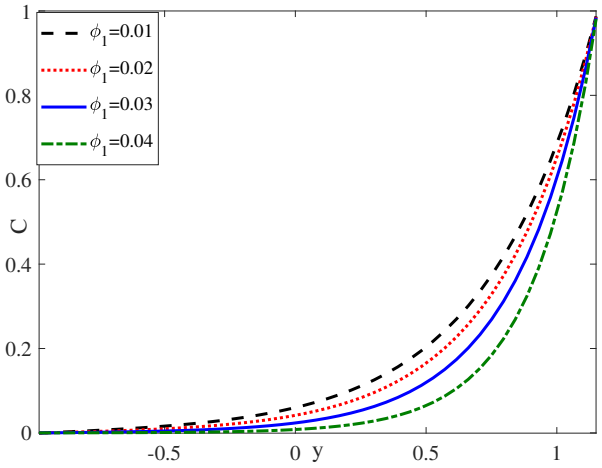

Fig. 13: Concentration distribution for different values of ϕ_1 when t= 0.1, Sc= 1, Kr= 1, $\phi_2 = 0.04$.

The Fig 11 and Fig 13 depict the temperature and concentration distribution of volume fraction ϕ_1. It is noted that the temperature increases with increases in the values of volume fraction, whereas the concentration profile decreases with an increase in values of volume fraction. This is due to the viscosity present in the nanoparticles, which shows shear thinning behavior at the highest concentration. Timofeeva et al. [42] have experimentally shown this. In Fig 12, it is observed that the temperature falls when the heat source parameter is increased. The concentration profile for different values of the chemical radiation parameter Kr is observed in Fig 14. It shows that concentration decreases with increases in the chemical reaction parameter. Moreover, the buoyancy effects are very important at the channel. It can also be said as fluid motion is retarded on account of the chemical reaction. When Kr $>$ 0, it leads to a fall in the concentration fluid, weakening the buoyancy effect due to the concentration gradient. Fig 15 depicts the concentration profile for various values of the Schmid number. It is noticed that the effect of increasing values of the Sc decreases the concentration distribution across the boundary layer. Physically, the rise in various values of Sc number leads to a reduction of molecular diffusion. Therefore, the concentration of the species is advanced for smaller values of Sc and lesser for larger values of Sc.

Fig16, Fig17, Fig 18 and Fig 19 depict the rate of heat transfer on Peclet number, heat source, thermal radiation parameter, and volume fraction ϕ. The below-given values are considered for calculation Pe = 10, Gr= 1, Gc= 1, Sc= 1, N= 1, Kr= 1, K= 1, $\beta = 2$, M= 1, ω= $\pi/4$, λ = 1. while other parameters are varied over a range which is listed in figure captions. Fig 16 displays the variation of heat transfer rate Nu with Peclet number over the channel walls $y = h_1$ and $y = h_2$. It is noticed that the heat transfer rate at $y = h_1$ increases due to an increase in Peclet number, whereas the reverse effect is observed at $y = h_2$. The rate of heat transfer on thermal radiation and volume fraction in Fig17, Fig 18, and Fig 19 varies periodically because of the asymmetric surface motion over the boundaries.

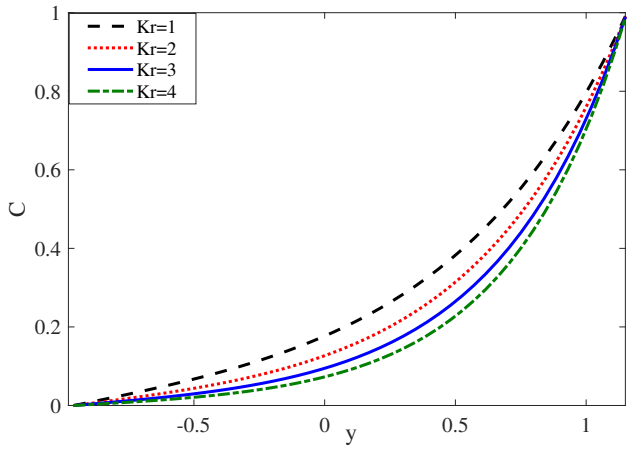

Fig. 14: Concentration distribution for different values of Kr when t= 0.1, Sc= 1, Kr= 1, $\phi_1 = 0.04$, $\phi_2 = 0.04$.

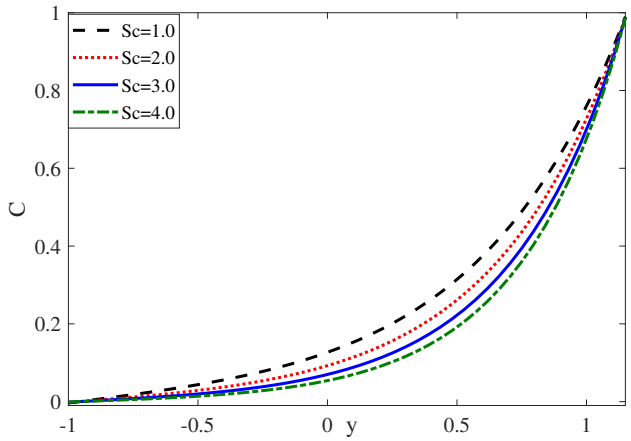

Fig. 15: Concentration distribution for different values of Sc when t= 0.1, Kr= 1, λ= 1, $\phi_1 = 0.04$, $\phi_2 = 0.04$.

Fig 20 and Fig 21 show the time series of skin friction and Sherwood number of different values of β Casson parameter and chemical reaction parameter, respectively. It is observed that skin friction and Sh vary periodically due to the asymmetric surface motion of fluid over boundaries. In Fig 22, the time series of skin friction of various values of permeability had been observed and it also varies periodically. Fig 23 displays the variation of Sherwood number Sh with various values of chemical reaction parameters at $y = h_1$ and $y = h_2$. It is found that Sh at $y = h_1$ raise with and is reversed at $y = h_2$ for various values of Kr.

B. Oscillatory flow analysis

Oscillatory parameters play a pivotal role in various scientific and engineering domains by characterizing the dynamic behavior of systems that exhibit periodic motion. These parameters, such as frequency, amplitude, and phase, are essential in understanding and analyzing oscillations, which are prevalent in fields ranging from physics and electronics to biology and signal processing. The study of oscillatory behavior enables us to comprehend natural phenomena

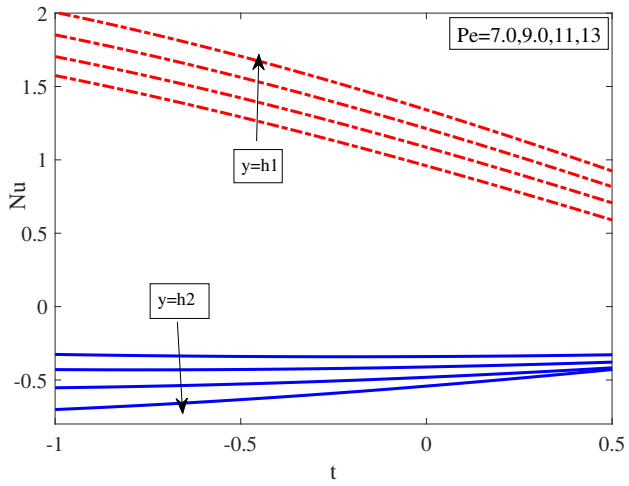

Fig. 16: Effect of Pe on Nusselt number when Pe=10, Gr= 1, N=1, $\beta = 2$, λ = 1, $\phi_1 = 0.04$, $\phi_2 = 0.04$.

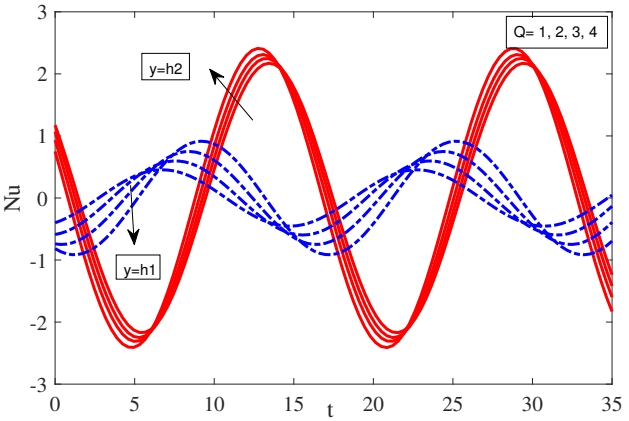

Fig. 17: Effect of Q on Nusselt number when Pe= 10, Gr= 1, N= 1, $\beta = 2$, λ = 1, $\phi_1 = 0.04$, $\phi_2 = 0.04$.

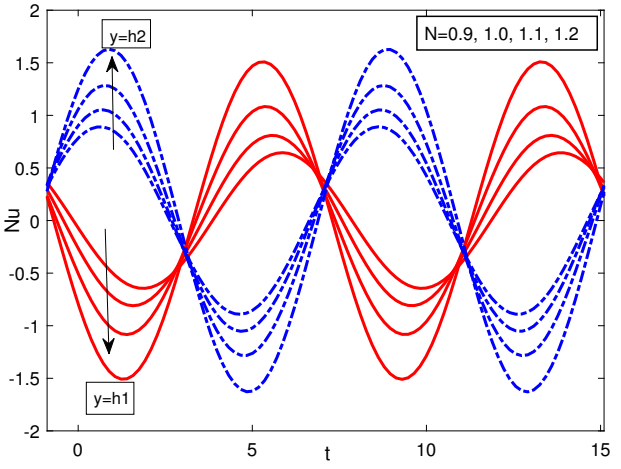

Fig. 18: Effect of N on Nusselt number when Gr= 1, Pe= 10, $\beta = 2$, λ= 1, $\phi_1 = 0.04$, $\phi_2 = 0.04$.

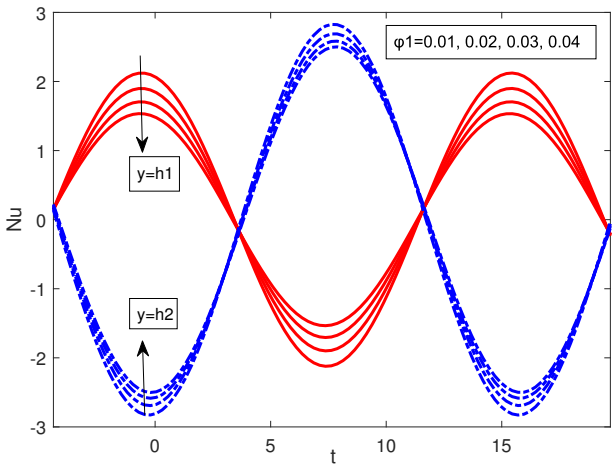

Fig. 19: Effect of ϕ_1 on Nusselt number when Gr= 1, N= 1, Pe=10, $\lambda = 1$ K= 1, $\beta = 2$, λ= 1.

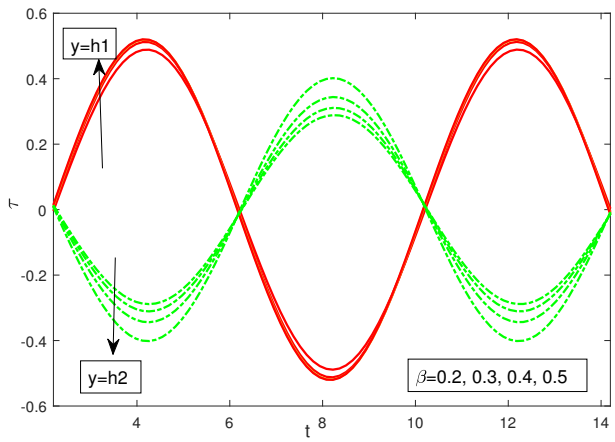

Fig. 20: Skin friction for various values of β when Gr= 1, N= 1, K= 1, M= 1, λ= 1, Q= 1, Sc= 1.

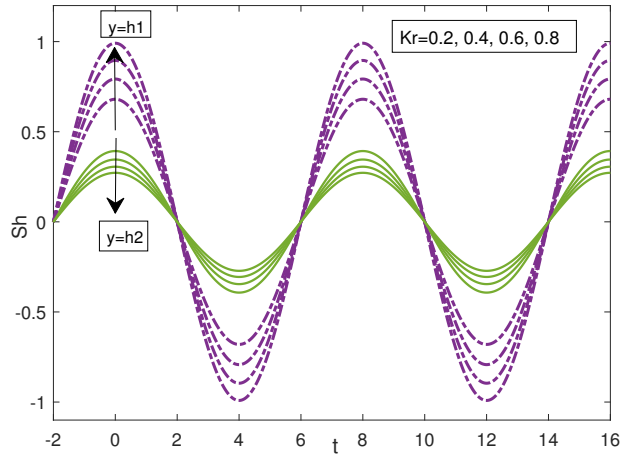

Fig. 21: Effect of Kr on Sherwood number when M= 1, Gr= 1, N = 1, K= 1, $\beta = 2$, λ= 1.

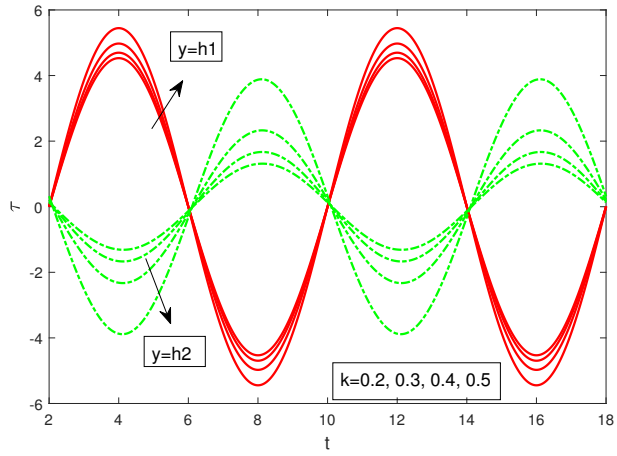

Fig. 22: Skin friction for various values of porosity k when M= 1, Gr= 1, N= 1, Kr= 1, $\beta = 2$, λ= 1.

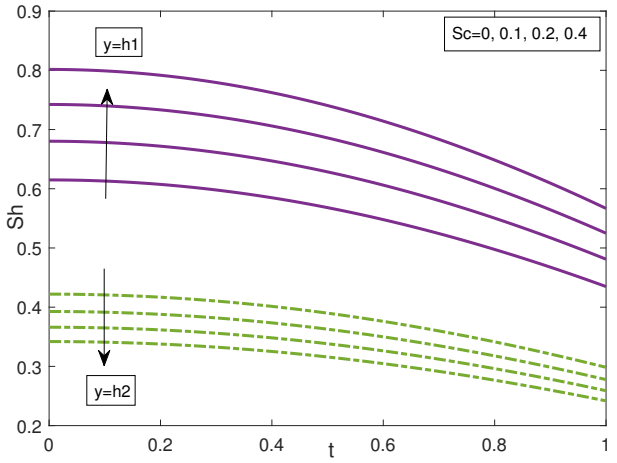

Fig. 23: Effect of Sc on Sherwood number when Kr= 1, $\beta = 2$, λ= 1.

like sound waves, electromagnetic signals, and biological rhythms, as well as design and optimize technologies such as communication systems, medical devices, and structural components. The velocity profile for various values of the oscillatory parameter (ω) is analysed in Fig 24. It is clear in the figure that the velocity decreases with an increase in the oscillatory parameter. This result is compared with Sasikumar et al. [32] and confirmed. The effect of the oscillatory parameter in the temperature profile has been analysed in Fig 25. It is noted that for various values of the oscillatory parameter, the temperature increases gradually from the left wall to the right wall. Fig 26 the velocity profile various values os asymmetric parameter has been analysed. It is noticed that the velocity trend is high when ($\phi = 3\pi/2$), followed by ($\phi = 3\pi/2$) and ($\phi = zero$). Fig 27 show the time series of skin friction for various values of asymmetric parameter (ϕ). It is observed that skin friction vary periodically due to the asymmetric surface motion of fluid over boundaries.

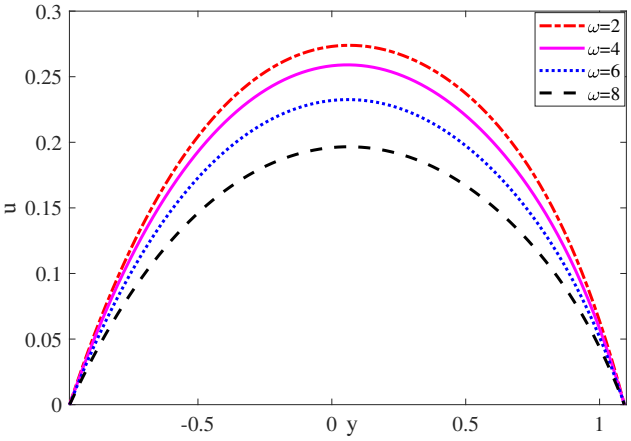

Fig. 24: Velocity distribution for different values of ω when t= 0.1, Pe= 10, Gr= 1, Gc= 1, M= 1, Kr= 1, k= 1, $\beta = 2$, M= 1, λ= 1, $Re = 1$, $Q = 1$.

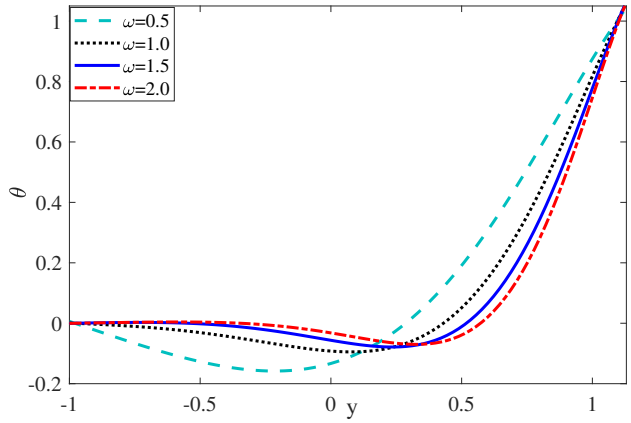

Fig. 25: Temperature distribution for different values of ω when t= 0.1, Pe= 10, N= 1, $\beta = 2$, $Q = 1$, $\phi_1 = 0.04$, $\phi_2 = 0.04$.

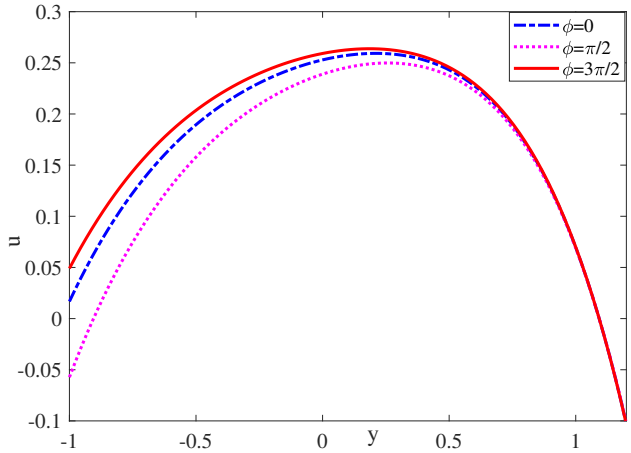

Fig. 26: Velocity distribution for different values of Asymmetric parameter when t= 0.1, Pe= 10, N= 1, $\beta = 2$, $Q = 1$, $\phi_1 = 0.04$, $\phi_2 = 0.04$.

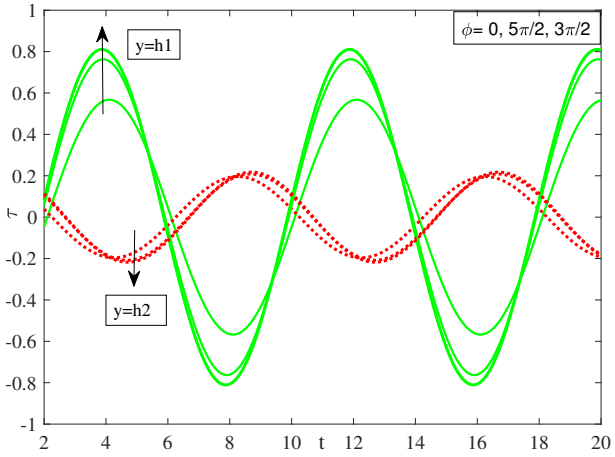

Fig. 27: Skin friction for various values of Asymmetric parameter when t= 0.1, Pe= 10, N= 1, $\beta = 2$, $Q = 1$, $\phi_1 = 0.04$, $\phi_2 = 0.04$.

C. Comparative results of skin friction coefficient and heat transfer rate for Cu-mixture

Copper (Cu) possesses exceptional heat conductivity. When combined with other materials as Cu-mixtures ($Cu - TiO_2, Cu - Al_2O_3$ and $Cu - SiO_2$), the overall thermal conductivity of the mixture is influenced by both copper and the added oxide components (TiO_2, Al_2O_3, or SiO_2)[25]. In certain Cu mixtures, the addition of specific oxides, such as alumina (Al_2O_3), can significantly enhance the overall thermal conductivity compared to pure copper. This enhancement makes Cu mixtures more efficient in transferring heat, rendering them suitable for diverse thermal management applications. Cu-mixtures find applications in various industries, including electronics, automotive, aerospace, and energy. They are utilized in components like heat exchangers, electrical connectors, cooling systems, and power electronics to facilitate the efficient transfer and management of heat. There is a unique combination of properties in the Cu-mixtures due to different oxides (TiO_2, Al_2O_3, and SiO_2). Various fields, including electronics, catalysis, thermal management, and electrical insulation, can use each mixture for a specific application because it has unique combination of properties. Specific Cu-mixtures can vary depending on the application and the desired balance of properties, including thermal and electrical conductivity, mechanical strength, thermal stability, and chemical resistance. The Cu-mixtures offer a wide range of advantages and unique features, making them valuable materials for numerous applications in various industries.

TABLE II: The Nusselt number for various values of heat generation/ absorption for different types of hybrid nanofluid when t= 0.1, Pe= 10, N=1.5, λ= 0.1, $M = 1$, $\omega = \pi/4$.

	Nusselt number		
Q	**Cu − TiO_2**	**Cu − Al_2O_3**	**Cu − SiO_2**
1	0.3856	0.3845	0.3974
2	0.2312	0.2371	0.2211
3	0.0509	0.0668	0.0162
4	-0.1831	-0.1582	-0.2305

TABLE III: The Nusselt number for various values of peclet number for different types of hybrid nanofluid when t= 0.1, Q= 1, N=1.5, λ= 0.1, $M = 1$, $\omega = \pi/4$.

	Nusselt number		
Pe	$\mathbf{Cu - TiO_2}$	$\mathbf{Cu - Al_2O_3}$	$\mathbf{Cu - SiO_2}$
7	0.2141	0.2075	0.2384
8	0.2806	0.277	0.2972
9	0.3363	0.3343	0.3493
10	0.3856	0.3845	0.3974

In general, the hybrid nanofluids with $Cu - SiO_2$, $Cu - TiO_2$, and $Cu - Al_2O_3$ nanoparticles offer the potential to enhance heat transfer due to their improved thermal conductivity, surface properties, and stability in the base fluid. However, the nanoparticle's specific performance and effectiveness in heat transfer applications can depend on various factors, such as nanoparticle concentration, size, shape, and material properties, as well as the base fluid characteristics and some effects.

The heat transfer rate for different hybrid nanofluids with varying heat generation/absorption values is compared in Table II. It is observed that $Cu - SiO_2$ exhibits a higher heat transfer rate than $Cu - TiO_2$ and $Cu - Al_2O_3$, especially when $Q = 1$. The lower heat generation/ absorption indicates a better heat conduction rate. Positive heat transfer values indicate that heat is being transferred in the expected direction, from a hotter region to a cooler region. Positive values indicate that a tremendous amount of heat is being transferred.

The heat transfer rate for different hybrid nanofluids with varying values of Peclet number is compared in Table III. Comparing the Peclet number values for each type of hybrid nanoparticle, the increasing values of the Peclet number raise the heat transfer rate. A higher Peclet number suggests a relatively more vital convective heat transfer component than conductive heat transfer. It can be concluded that $Cu - SiO_2$ has a high heat transfer rate, followed by $Cu - TiO_2$ and $Cu - Al_2O_3$ when the heat generation/ absorption values and Peclet number increase.

TABLE IV: The Skin Friction Coefficient for various values of magnetic field parameter for different types of hybrid nanofluid when t= 0.1, Pe= 10, λ= 0.1, $N = 1$, $\omega = \pi/4$.

	Skin Friction Coefficient		
M	$\mathbf{Cu - TiO_2}$	$\mathbf{Cu - Al_2O_3}$	$\mathbf{Cu - SiO_2}$
1	-2.0697	-2.1044	-2.042
2	-1.9156	-1.9252	-1.9137
3	-1.8723	-1.8761	-1.883
4	-1.8352	-1.8367	-1.8523

TABLE V: The Skin Friction Coefficient for various values of chemical reaction parameter for different types of hybrid nanofluid when t= 0.1, Pe= 10, λ= 0.1, $N = 1$, $\omega = \pi/4$.

	Skin Friction Coefficient		
Kr	$\mathbf{Cu - TiO_2}$	$\mathbf{Cu - Al_2O_3}$	$\mathbf{Cu - SiO_2}$
0.2	-5.5243	-5.2517	-5.0715
0.4	-0.3062	-0.6115	-0.5213
0.6	-2.9932	-3.0804	-3.1974
0.8	-2.8334	-2.8683	-2.9548

The Skin friction coefficient for different hybrid nanofluids with varying magnetic field parameters and chemical reaction parameters in Table IV and Table V respectively, is investigated. As the magnetic field parameters increase, the skin friction coefficient decreases. This has potential benefits in terms of reducing friction and improving the efficiency of the Cu-mixture. At each magnetic field parameter value, the variations in the skin friction coefficient among the Cu-mixture is observed. $Cu - TiO_2$ exhibits the highest skin friction coefficient, followed by $Cu - Al_2O_3$, and $Cu - SiO_2$ has the lowest skin friction coefficient across the magnetic field parameters. This comparison indicates that $Cu - SiO_2$ is the most favorable material in reducing friction, especially when subjected to a magnetic field. In Table V, as the chemical reaction parameter increases, the skin friction coefficient also increases. It is observed that $Cu - TiO_2$ shows the lowest reaction for τ, followed by $Cu - Al_2O_3$, and $Cu - SiO_2$ has the highest reaction value. The fluctuations in the chemical reaction parameter are attributed to the interactions between the materials and the reaction parameter.

D. Validation of the results

To validate the study a comparison of Skin Friction Coefficient, Heat transfer rate and Mass transfer rate is calculated using Bvp4c and Exact solution for $Cu - TiO_2$.
The values of skin-friction coefficient, Nusselt number and Sherwood number are given in Table VI, Table VII and TableVIII for different values of the physical parameters, namely k; M; R; Q; ω; N; Pe and Kr. The comparison has been carried out using Bvp4c and the exact solution for the above-mentioned tabled. In Table VI, it is observed that an increase in M or Gr decreases the rate of skin friction coefficient, whereas a rise in ω or k increases it. Also, in Table VII rise in values of Pe or ω or Q enhances the rate of heat transfer, but a rise in thermal radiation decreases it. Likewise, in Table VIII, it is noticed that a rise in the chemical reaction parameter or Schmid number enhances the rate of mass transfer, whereas the oscillatory parameter ω decreases the Sherwood number. Table IX displays the comparison of Sherwood number for different values of chemical reaction parameter with the results of Satya Narayanan et al. [31] by omitting the nanoparticle terms. The results show an excellent agreement. From Table VI, VII and VIII, it can be noticed that the numerical values for skin friction coefficient, Nusselt number and Sherwood number are approximately the same with Exact solution.

TABLE VI: Skin-friction variations for various parameters when t= 0.1, Pe= 10, Gr= 1, Gc=1, N= 1, Kr= 1,k= 1, $\beta = 2$, λ= 1, $Re = 1$, $M = 1$, $\omega = \pi/4$.

M	k	ω	Gr	$\tau(Exact)$	$\tau(Numerical)$
0.5	2	pi/4	1	1.5587	1.5517
1				1.4003	1.4069
1.5				1.2598	1.2411
2				1.1461	1.1407
	1			0.9486	0.8243
	1.5			0.9167	0.7802
	2			0.8874	0.8504
		0.1		4.3899	4.3957
		0.2		4.4301	4.4319
		0.3		4.4886	4.4923
		0.4		4.5722	4.5767
			1	5.1127	5.1271
			2	7.8294	7.8303
			3	10.5417	10.5389
			4	13.2412	13.2448

TABLE VII: Nusselt Number variations for various parameters when t= 0.1, Pe= 10, N=1, λ= 1, $M = 1$, $\omega = \pi/4$.

N	Pe	ω	Q	$Nu(Exact)$	$Nu(Numerical)$
0.1	10			1.7591	1.7622
0.2				2.0888	2.0899
0.3				2.4795	2.4887
0.4				2.9812	2.9875
	7			1.3432	1.3694
	8			1.4663	1.4869
	9			1.5777	1.6043
	10			1.9716	2.0503
		0.1		0.7680	0.7462
		0.2		1.0502	1.0352
		0.3		1.3675	1.2835
		0.4		1.5221	1.4816
			0.1	0.7078	0.7060
			0.2	0.8621	0.8664
			0.3	1.0501	1.0466
			0.4	1.2517	1.2513

TABLE VIII: Sherwood Number variations for various parameters when t= 0.1, Kr= 1, $\beta = 2$, $Sc = 1, \omega = \pi/4$.

kr	Sc	ω	$sh(Exact)$	$sh(Numerical)$
0.2			-0.5397	-0.5387
0.4			-0.6641	-0.6623
0.6			-0.7795	-0.7748
0.8			-0.8758	-0.8782
	0.5		-0.7421	-0.7498
	1		-0.7106	-0.7198
	1.5		-0.6879	-0.6898
	2		-0.6525	-0.6599
		0.1	-0.7891	-0.7811
		0.2	-0.7792	-0.7781
		0.3	-0.7747	-0.7730
		0.4	-0.7683	-0.7660

TABLE IX: Comparison of sherwood number calculated using Bvp4c for satya narayanan et al.[31] for t= 0.1, Sc=0.16, Gr= 1, Gc=1, N= 0.5, Kr= 1, $\beta = 2$, Pe= 0.1, λ= 0.1, $Re = 0.1$, $M = 1$.

Kr	$Present$	$SatyaNarayana$[31]
0.2	0.4792	0.48343
0.4	0.4831	0.48544
0.6	0.4838	0.4875
0.8	0.4922	0.48962

V. CONCLUSION

The effect of the chemical reaction and heat generation/ absorption in MHD oscillatory flow in $CuTiO_2/H_2O$ Casson hybrid nanofluid flow in an irregular wavy channel in the presence of a magnetic field is investigated. The governing PDEs are transformed into ODEs and exact solutions are obtained. For various flow parameters, MATLAB software is used to generate velocity, temperature, and concentration profiles.

- An increase in M, Kr, β, ω, and Re decreases the velocity field, whereas an increase in Gr, k and N enhances the velocity field.
- An enhancement in heat generation/absorption parameter reduces the temperature distribution and from y=0.6, it gradually increases the temperature.
- The concentration field of the fluid decreases with an increase in Sc, Kr and ϕ_1.
- The skin friction coefficient raises when β increases at $y = h_1$ while it has the opposite effect at $y = h_2$.
- The Sherwood number increases when the chemical reaction parameter increases at $y = h_1$ and it is reversed at $y = h_2$.
- The comparison of heat transfer rates among water-based nanofluids, namely $Cu - SiO_2$, $Cu - TiO_2$, and $Cu - Al_2O_3$, reveals that $Cu - SiO_2$ exhibits superior performance. This is particularly evident when there is an increase in the values of heat generation/absorption and Peclet number.

VI. NOMENCLATURE

a_1, b_1	Amplitudes of irregular channel
a, b	Empirical shape factor
B_0	Electromagnetic induction
$d_1 + d_2$	Width of channel
B_0	Magnetic field intensity
d	Mean half width of channel
Gr	Grashof number
Pe	Peclet number
u	Axial velocity
K	Porous medium
k_{nf}	Thermal conductivity
p	Dimensionless fluid pressure
q	Radiative heat flux
$(c_p)_s$	Specific heat capacitance of solid Np
$(c_p)_f$	Specific heat capacitance of base fluid
t	Time
H_1, H_2	wall condition
$h_1,\ h_2$	Channel walls
N	Thermal radiation parameter
Nu	Nusselt number

	Greek Symbols
α	Mean radiation absorption coefficient
ρ_f	Densities of base fluid
ρ_s	Densities of solid nanoparticle
ρ_{nf}	Density of nanofluid
μ_{nf}	Dynamic viscosity of Nf
$(\rho\beta)_{nf}$	Thermal expansion of Nf
ρc_p	Heat capacitance of Nf
β_s	Volumetric coeff. of thermal expansion
β_f	Volumetric coeff. of thermal expansion
σ	Electrical conductivity
ϕ	Volume fraction
θ	Fluid temperature
λ	Pressure gradient
τ	Skin friction at the wall
ω	Frequency of the oscillation

VII. APPENDIX

$$\begin{array}{ll} l^2 & = \psi_2(1+\frac{1}{\beta}) \\ s^2 & = \psi_1 Re + M + \frac{\psi_2}{k} \\ p^2 & = \frac{N^2+Q-\psi_5 Pei\omega}{\lambda_{hnf}} \\ r^2 & = kr + \frac{Sc}{1-\phi} \\ A1 & = \frac{\lambda l^2}{s^2} \\ B1 & = \frac{\psi_3 Grl^2}{p^2 l^2 + s^2} \\ C1 & = \frac{\psi_4 Gml^2}{r^2 l^2 + s^2} \end{array}$$

ACKNOWLEDGMENT

I would like to express my deep gratitude to the management and Department of Mathematics of SRM Institute of Science and Technology for giving me the opportunity to conduct this research at this university.

REFERENCES

[1] Choi S.U.S., "Enhancing thermal conductivity of fluids with nanoparticle", In: D.A. Siginer, H.P. Wang (Eds.), Developments and Applications of Non-Newtonian Flows, The ASME New York. FED Vol.231/MD Vol.66, pp. 99-105,1995.

[2] Hasnain, J., Abid, N., Alansari, M. O., and Ullah, M. Z., "Analysis on Cattaneo-Christov heat flux in three-phase oscillatory flow of non-Newtonian fluid through porous zone bounded by hybrid nanofluids", Case Studies in Thermal Engineering, 102074, 2022.

[3] D. Madhesh, R. Parameshwaran and S. Kalaiselvam, "Experimental investigation on convective heat transfer and rheological characteristics of $Cu - TiO_2$ hybrid Nanofluids", Experimental Thermal and Fluid Science , 52, 104–115, 2014.

[4] Naheeda Iftikhar, Abdul Rehman, Hina Sadaf, "Theoretical investigation for convective heat transfer on Cu/water nanofluid and (SiO_2-copper)/water hybrid nanofluid with MHD and nanoparticle shape effects comprising relaxation and contraction phenomenon", International Communications in Heat and Mass Transfer 120, 105012, 2021.

[5] Gul Aaiza, Ilyas Khan, and Sharidan Shafie, "Energy Transfer in Mixed Convection MHD Flow of Nanofluid Containing Different Shapes of Nanoparticles in a Channel Filled with Saturated Porous Medium", Nanoscale Research Letters, 10:490, 2015.

[6] Mustafa M, Hayat T, Pop I, Aziz A, "Unsteady boundary layer flow of a Casson fluid due to an impulsively started moving flat plate", Heat Transfer – Asian Res , 40(6):563–76, 2011.

[7] Bhattacharyya K, Hayat T, Alsaedi A, " Analytic solution for magnetohydrodynamic boundary layer flow of Casson fluid over a stretching/shrinking sheet with wall mass transfer", Chin Phys B 22(2):024702, 2013.

[8] Fung YC, " Biodynamics circulation", New York Inc: Springer Verlag, 1984.

[9] Nadeem S, Ul Haq R, Lee C, " MHD flow of a Casson fluid over an exponentially shrinking sheet", Sci Iran 19(6):1550–3, 2012.

[10] Kandasamy A, Pai RG, "Entrance region flow of casson fluid in a circular tube", Appl Mech Mater 110–116:698–706, 2012.

[11] Eldabe, N. T. M., G. Saddeck, and A. F. El-Sayed. "Heat transfer of MHD non-Newtonian Casson fluid flow between two rotating cylinders", Mechanics and Mechanical Engineering 5.2: 237-251, 2001.

[12] Mukhopadhyay, S., De, P. R., Bhattacharyya, K., and Layek, G. C, "Casson fluid flow over an unsteady stretching surface", Ain Shams Engineering Journal, 4(4), 933-938, 2013.

[13] Hari R. Kataria , Harshad R Patel, "Soret and heat generation effects on MHD Casson fluid flow past an oscillating vertical plate embedded through porous medium", Alexandria Engineering Journal 55, 2125–2137, 2016.

[14] G. Jithender Reddy, R. Srinivasa Raju , J. Anand Rao," Influence of viscous dissipation on unsteady MHD natural convective flow of Casson fluid over an oscillating vertical plate via FEM", Ain Shams Engineering Journal 9 1907–1915, 2018.

[15] Sidra Aman, Syazwani Mohd Zokri, Zulkhibri Ismail, Mohd Zuki Salleh, Ilyas Khan, "Effect of MHD and Porosity on Exact Solutions and Flow of a Hybrid Casson-Nanofluid", Journal of Advanced Research in Fluid Mechanics and Thermal Sciences 44, Issue 1, 131-139, 2018.

[16] Zahir Shah, Poom Kumam and Wejdan Deebani , "Radiative MHD Casson Nanofluid Flow with Activation energy and chemical reaction over past nonlinearly stretching surface through Entropy generation", Scientific Reports, 10:4402, 2020.

[17] Liu, Yaqing, Liancun Zheng, Xinxin Zhang, and Fenglei Zong. "The oscillating flows and heat transfer of a generalized Oldroyd-B fluid in magnetic field." IAENG International Journal of Applied Mathematics, vol. 40, no.4, pp276-281, 2010.

[18] Zainal Abdul Aziz, Faisal Salah, and Dennis Ling Chuan Ching, " On accelerated flow for MHD generalized burgers' fluid in a porous medium and rotating frame", IAENG International Journal of Applied Mathematics, vol. 41, no. 3,pp199-205, 2011.

[19] Sasikumar, J., Bhuvaneshwari, S., Govindarajan, A., " Diffusion of chemically reactive species in MHD oscillatory flow with thermal radiation in the presence of constant suction and injection", In Journal of Physics: Conference Series, IOP Publishing, Vol. 1000, No. 1, p. 012033, 2018.

[20] Colla L, Fedele L, Scattolini M, Bobbo S ," Water-based Fe_2O_3 nanouid characterization: thermal conductivity and viscosity measurements and correlation", Advances in Mechanical Engineering, Article ID 674947:8, 2012.

[21] Zaheer Abbas, Sifat Hussain, Muhammad Y. Rafiq, Jafar Hasnain, "Oscillatory slip f low of Fe_3O_4 and Al_2O_3 nanoparticles in a vertical porous channel using Darcy's law with thermal radiation", Heat Transfer, 1–18, 2020.

[22] Labib, M. Nuim, Md J. Nine, Handry Afrianto, Hanshik Chung, and Hyomin Jeong. "Numerical investigation on effect of base fluids and hybrid nanofluid in forced convective heat transfer", International Journal of Thermal Sciences, 71 (2013): 163-171, 2013.

[23] Hayat, Tanzila, S. Nadeem, and A. U. Khan, "Numerical analysis of Ag–CuO/water rotating hybrid nanofluid with heat generation and absorption", Canadian Journal of Physics 97, no. 6 : 644-650, 2019.

[24] Iqbal, Z., Akbar, N.S., Azhar, E. and Maraj, E.N., "Performance of hybrid nanofluid (Cu-CuO /water) on MHD rotating transport in oscillating vertical channel inspired by Hall current and thermal radiation", Alexandria Engineering Journal, Vol. 57, pp. 1943-1954, 2018.

[25] Gupta Shipra Mital and Tripathi Manoj, "A review of TiO_2 nanoparticles", Chines science bulletin, Vol.56 No.16: 1639–1657, 2011.

[26] Ali J. Chamkha ,S. Abbasbandy ,A.M. Rashad and K. Vajravelu, "Radiation effects on mixed convection about a cone embedded in a porous medium filled with a nanofluid.", Meccanica, 48:275–285, 2013.

[27] R. L. Hamilton and O.K Crosser, "Thermal conductivity of heterogeneous two-component systems", American Chemical Society, Vol. 1 No 3, August 1962.

[28] Samuel Olumide Adesanya, Oluwole Daniel Makinde, "Mhd oscillatory slip flow and heat transfer in a channel filled with porous media", U.P.B. Sci. Bull., Series A, Vol. 76, Iss. 1, 2014.

[29] V. Zin, F. Agresti1, S. Barison, L. Colla, and M. Fabrizio, "Influence of Cu, TiO_2 Nanoparticles and Carbon Nano-Horns on Tribological Properties of Engine Oil", Journal of Nanoscience and Nanotechnology, Vol. 15, 3590–3598, 2015.

[30] Narayana, P. S., Venkateswarlu, B., and Devika, B. , "Chemical reaction and heat source effects on MHD oscillatory flow in an irregular channel", Ain Shams Engineering Journal, 7(4), 1079-1088, 2016.

[31] Sasikumar, J., and Govindarjan, A, "Effect of Heat and Mass transfer on MHD Oscillatory flow with Chemical reaction and slip conditions in asymmetric wavy channel". ARPN Journal of Engineering and Applied Sciences, 11, 1164-1170, 2016.

[32] S. Asghar, M. R. Mohyuddin, T. Hayat, And A. M. Siddiqui, "The Flow Of A Non-Newtonian Fluid Induced Due To The Oscillations Of A Porous Plate", Mathematical Problems in Engineering, 2 133–143, 2004.

[33] O. D. Makinde and P. Y. Mhone," Heat Transfer to Mhd Oscillatory Flow In A Channel Filled With Porous, Medium", Rom. Journ. Phys., Vol. 50, Nos. 9–10, P. 931-938, Bucharest, 2005.

[34] Mutuku, W. N, " Ethylene glycol (EG)-based nanofluids as a coolant for automotive radiator", Asia Pacific Journal on Computational Engineering, 3(1), 1-15, 2016.

[35] Sasikumar, J., Harinisha, N., Anitha, S, "MHD oscillatory flow through porous medium in rotating wavy channel with heat source", In AIP Conference Proceedings AIP Publishing LLC, Vol. 2112, No. 1, p. 020104, 2019.

[36] Sasikumar, J., Anitha, S., Harinisha, N, "Effect of velocity slip on MHD periodic flow through irregular channel", In AIP Conference Proceedings AIP Publishing LLC, Vol. 2277, No. 1, p. 030021, 2020.

[37] Sasikumar J, Senthamarai R. "Chemical reaction and viscous dissipation effect on MHD oscillatory blood flow in tapered asymmetric channel", Mathematical Modeling and Computing , 10.23939/mmc2022.04.999, 2022.

[38] Itishree Nayak, "Numerical Study of MHD Flow and Heat Transfer of an Unsteady Third Grade Fluid with Viscous Dissipation," IAENG International Journal of Applied Mathematics, vol. 49, no.2, pp245-252, 2019.

[39] Hamzeh T. Alkasasbeh, Mohammed Z. Swalmeh, Abid Hussanan, and Mustafa Mamat, "Numerical Solution of Heat Transfer Flow in

Micropolar Nanofluids with Oxide Nanoparticles in Water and Kerosene Oil about a Horizontal Circular Cylinder," IAENG International Journal of Applied Mathematics, vol. 49, no.3, pp326-333, 2019.

[40] Faisal Salah, and Mubarak H. Elhafian, "Numerical Solution for Heat Transfer of Non - Newtonian Second - Grade Fluid Flow over Stretching Sheet via Successive Linearization Method," IAENG International Journal of Applied Mathematics, vol. 49, no.4, pp505-512, 2019.

[41] Dipen Saikia, Utpal Kumar Saha, and G. C. Hazarika, "A Numerical Study of Atangana-Baleanu and Caputo-Fabrizio for MHD Flow Problem over a Vertical Hot Stretching Sheet with Variable Viscosity and Thermal Conductivity," IAENG International Journal of Applied Mathematics, vol. 50, no.3, pp616-627, 2020.

[42] Susanta Maity, Palky Handique, and Swatilekha Nag, "Unsteady Thin Liquid Film Flow on a Porous Stretching Cylinder," IAENG International Journal of Applied Mathematics, vol. 52, no.1, pp213-218, 2022.

[43] Devaki B, Sampath Kumar V S, and Nityananda P Pai, "Analysis of Casson Flow Through Parallel and Uniformly Porous Walls of Different Permeability," IAENG International Journal of Applied Mathematics, vol. 53, no.1, pp9-16, 2023.

[44] Faisal Salah, Zainal Abdul Aziz, and Dennis Ling Chuan Ching, "On accelerated MHD flows of second grade fluid in a porous medium and rotating frame", IAENG International Journal of Applied Mathematics, 43(3), 106-113, 2013.

[45] P. Vaidehi, and J. Sasikumar, "Darcy Flow of unsteady Casson Fluid subject to thermal radiation and Lorentz force on wavy walls: Case of Slip flow for small and large values of plastic dynamic viscosity." Thermal Science and Engineering Progress: 101885, 2023.

[46] Barkilean, J., Jagadeesan, S. "Heat transfer characteristics on MHD oscillatory radiative nanofluid with $H_2O/C_2H_6O_2$ (Basefluid): A comparative study of different nanoparticles of various shapes," International Journal of Heat and Technology, Vol. 41, No. 3, pp. 529-540, 2023.